Inorganic Chemistry

ARTICLE

pubs.acs.org/IC

Large Thermal Conductivity Reduction Induced by La/O Vacancies in the Thermoelectric $LaCoO_3$ System

Yang Wang,[*,†,‡] Fang Li,[§] Luxiang Xu,[∥] Yu Sui,[*,†,⊥] Xianjie Wang,[†] Wenhui Su,[†] and Xiaoyang Liu[¶]

[†]Center for Condensed Matter Science and Technology (CCMST), Department of Physics, Harbin Institute of Technology, Harbin 150001, China

[‡]Division of Physics and Applied Physics, School of Physical and Mathematical Sciences, Nanyang Technological University, 21 Nanyang Link, 637371 Singapore, Singapore

[§]School of Petroleum Engineering, Southwest Petroleum University, Chengdu 610500, China

[∥]Lab for Low-dimensional Structure Physics, Institute of Solid State Physics and School of Physics and Electronic Engineering, Sichuan Normal University, Chengdu 610068, China

[⊥]International Center for Materials Physics, Academia Sinica, Shenyang 110015, China

[¶]State Key Laboratory of Inorganic Synthesis and Preparative Chemistry, College of Chemistry, Jilin University, Changchun 130012, China

Supporting Information

ABSTRACT: A series of compact La/O-vacant $La_{1-x}CoO_{3-y}$ compounds were prepared by a cold high-pressure procedure, and their thermoelectric (TE) properties were investigated. Compared with the ion-substituted hole-type $LaCoO_3$ systems (e.g., $La_{1-x}Sr_xCoO_3$), the thermal conduction of $La_{1-x}CoO_{3-y}$ is noticeably reduced by the La/O vacancies, whereas the electric transport is less influenced, which results in an efficient ZT enhancement. We demonstrate that the large thermal conductivity reduction originates from the strong point-defect scattering, and $La_{1-x}CoO_{3-y}$ can be rationalized as a partially filled solid solution: $La_{1-x}\square_xCoO_{3-y}\square_y$, where $\square$ denotes a vacancy. Such intrinsic thermal conductivity suppression provides an effective pathway for the design of better TE materials.

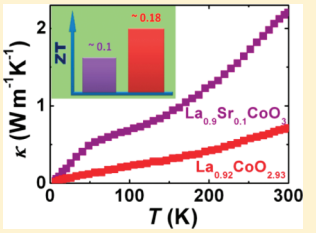

INTRODUCTION

About two-thirds of the energy we consume is lost during energy transportation, storage, transformation, and applications, mainly in the form of waste heat. Thermoelectric (TE) materials make it possible to generate electric energy from industry waste and other low-grade heat such as solar energy and geothermal energy. Some high-performance TE alloys have been used for electric generation and cooling. Recently, TE oxides have been attracting much attention because of their particular advantages and more extensive application potentials than conventional TE alloys.[1,2] Nevertheless, the TE efficiency in oxides is still at a lower level compared with that in TE alloys. The efficiency of a TE material is usually described by the figure of merit ZT, defined as $S^2T/\rho\kappa$, where S, T, ρ, and κ are thermopower, absolute temperature, resistivity, and thermal conductivity, respectively. The relatively large κ in oxides is one important reason for the lower ZT. For instance, S^2/ρ of the layered cobalt oxide $NaCo_2O_4$ is comparable to that of a state-of-the-art TE Bi_2Te_3 alloy, but its κ is much higher than that of Bi_2Te_3.[3,4] Another example is perovskite-type TE oxides: $SrTiO_3$ and $LaCoO_3$ systems.[5,6] In slightly electron-doped $SrTiO_3$ and hole-doped $LaCoO_3$, S^2/ρ is quite large among oxides, but ZT is still not competitive because of the high κ.[5,6] Therefore, reducing κ but keeping S^2/ρ unchanged is the key to improving the TE performance of oxides. Moreover, the strong coupling between S and ρ causes S and ρ to usually increase or decrease simultaneously, so it is difficult to noticeably increase S^2/ρ. Thus, suppression of κ is an effective means for enhancing ZT.

Nanostructuring provides an approach to improving ZT through phonon engineering and reduction of κ,[2] which has been achieved in types of TE semiconductors and alloys.[7,8] Nanostructures with one or more dimensions smaller than the mean free path of phonons but larger than that of electrons will strongly reduce κ without noticeably affecting electrical transport. However, intrinsic suppression of κ, which is independent of the sample morphology, is the root of developing TE materials. The search for materials with low κ and an understanding of the mechanism of κ reduction could be very helpful for the ongoing research on TEs.

In this study, we report the TE properties of La/O-vacant $La_{1-x}CoO_{3-y}$, which suggests an efficient pathway to reducing κ in oxides through the introduction of vacancies, with ρ and S remaining undisturbed. Our previous investigations on the $La_{1-x}Sr/Ca_xCoO_3$ systems indicate that $La_{1-x}Sr_xCoO_3$ has a better TE performance than $La_{1-x}Ca_xCoO_3$ and the optimal ZT exists at $x = 0.1$.[9] Therefore, herein we mainly present the results of $La_{0.92}CoO_{2.93}$ whose Co^{3+}/Co^{4+} ratio is identical with that of $La_{0.9}Sr_{0.1}CoO_3$ and compare the TE properties of $La_{0.92}CoO_{2.93}$ and $La_{0.9}Sr_{0.1}CoO_3$. In the following,

Received: December 22, 2010
Published: April 13, 2011

we will see that the same Co^{3+}/Co^{4+} ratio causes $La_{0.92}CoO_{2.93}$ and $La_{0.9}Sr_{0.1}CoO_3$ to have comparable electric transport properties, but the La/O vacancies in $La_{0.92}CoO_{2.93}$ strongly suppress thermal transport, which induces a significant *ZT* enhancement.

EXPERIMENTAL SECTION

Polycrystalline $La_{1-x}CoO_{3-y}$ ($x = 0-0.12$) samples were prepared by a solid-state reaction, followed by a cold high-pressure synthesis procedure. First, appropriate amounts of La_2O_3 and Co_3O_4 powders were mixed, pressed into pellets, and sintered in air at 1273−1373 K for 48 h with intermediate grindings. Then, the as-synthesized products were repeatedly ground into fine powders. Next, the powders were placed in a 6-mm-diameter hole drilled in the center of a gasket made of a dense, strong cardboard and loaded between two tungsten carbide anvils. Subsequently, the powders in the gasket were cold-pressed into pellets under a high pressure of 3 GPa with a special steel die for several minutes. (Note that the gasket was subjected to an average pressure of 3 GPa, but on the sample at the gasket center, the pressure may have been much higher.) After release of pressure, a thin, compact, pellet-shaped sample was obtained. The surface of these cold-pressed pellets shows a metallic shine. Finally, the samples were annealed at 1473 K for 24 h in a mixed gas (5% H_2/Ar).

Powder X-ray diffraction (XRD) data of the samples were collected using a XRD diffractometer (D8 Advanced) with Cu Kα ($\lambda = 0.154\,06$ nm) radiation. The data were collected from 10° up to 140° in 2θ with 0.02° steps and a counting time of 30 s per step. The XRD pattern of these samples, as shown in Figure 1, are consistent with that of pure $LaCoO_3$,[9] confirming that single-phase samples are successfully fabricated. The XRD refinement, by using the profile analysis program *Fullprof*, indicates that the $La_{1-x}CoO_{3-y}$ samples have smaller lattice parameters *a* than the stoichiometric $LaCoO_3$ (see Table 1), which suggests contraction of the lattice in $La_{1-x}CoO_{3-y}$.

The microstructure of the samples was observed by scanning electron microscopy (SEM; JEOL JSM-6700F), which reveals that these samples are quite dense, without any obvious pores and cracks; the typical grain size is 2−3 μm (see the inset of Figure 2a). The density of these samples is ∼7.10 g/cm^3, very close to the theoretical density (∼7.25 g/cm^3). The chemical composition of the samples was determined by energy-dispersive spectroscopy (EDS; JEOL JSM-6700F). Note that the probed region of the EDS measurement is on the scale of several hundred nanometers, much smaller than the grain size, so the probed volume is only a fraction of one grain and does not include amorphous, defect regions, boundaries, etc. Therefore, the element content can be obtained from EDS analysis. The atom percentage, Co^{3+}/Co^{4+} ratio, and oxygen content were further identified by X-ray photoelectron spectroscopy (XPS; ESCA 100-VSW) and iodometric titration. The results from these parallel experiments are consistent, so the chemical composition of the samples can be well determined. As an example of $La_{0.92}CoO_{2.93}$, the EDS result shows La:Co:O ≈ 0.9:1:2.95, the iodometric titration determines that the oxygen content is ∼2.93, and both XPS and titration results give $Co^{3+}:Co^{4+}$ = 9:1, which is identical with the cases of $La_{0.9}Sr_{0.1}CoO_3$ and $La_{0.9}Ca_{0.1}CoO_3$. Detailed EDS and XPS results are shown in the Supporting Information.

The TE properties (κ, ρ, and *S*), Hall coefficient, and specific heat were all measured by a physical property measurement system (Quantum Design). Resistivity and thermopower measurements were performed by a standard four-probe method, whereas the Hall coefficient was measured using a five-probe method with copper wire as leads. The thermal conductivity and specific heat were measured using a steady-state technique in a closed-cycle refrigerator pumped down to 10^{-5} Torr.

RESULTS AND DISCUSSION

The cold high-pressure procedure adopted in this study is the same as the method developed by Zhou et al.[10] As shown by

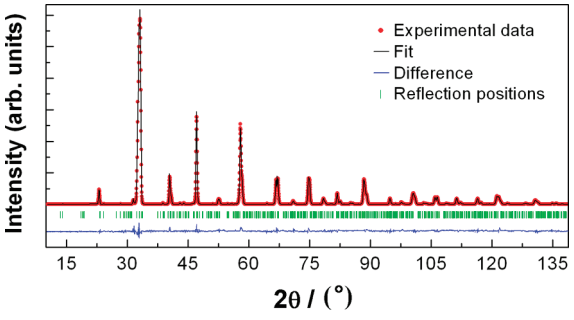

Figure 1. XRD pattern and Rietveld refinement result for $La_{0.92}CoO_{2.93}$ at room temperature. The experimental data are shown as red dots; the global fitting profile and the difference curve are shown as black and blue solid lines, respectively; the calculated reflection positions are indicated by green short sticks.

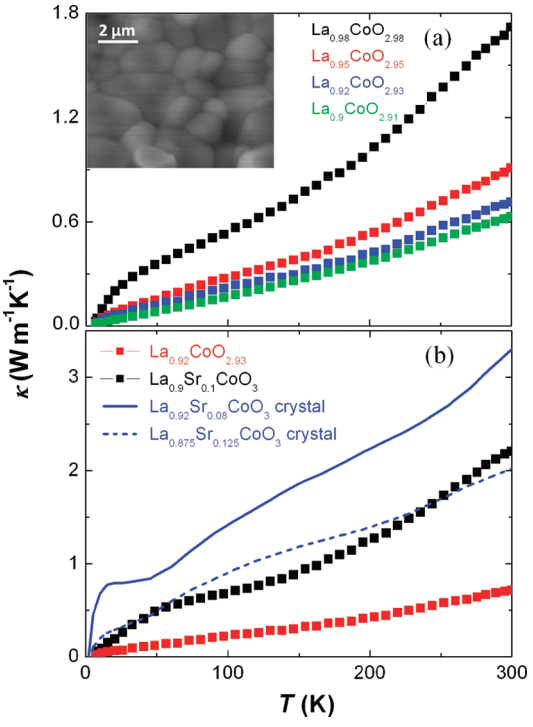

Figure 2. (a) Temperature dependence of thermal conductivity κ for the $La_{1-x}CoO_{3-y}$ samples. The inset shows a SEM image of a cross section of $La_{0.92}CoO_{2.93}$. (b) $\kappa(T)$ of $La_{0.92}CoO_{2.93}$ and $La_{1-x}Sr_xCoO_3$ samples. The κ data of $La_{0.92}Sr_{0.08}CoO_3$ and $La_{0.875}Sr_{0.125}CoO_3$ crystals are from ref 12.

Table 1. Room Temperature Lattice Parameters, Atomic Positions, Isotropic Thermal Factor B_{iso}, and Fitting Factors (R_{wp}, R_B, and R_F) for $LaCoO_3$ and $La_{0.92}CoO_{2.93}$ Based on a Rhombohedral $R\bar{3}c$ Space Group from the XRD Refinement

	a (Å)	*β* (deg)	B_{iso}(La) (Å^2)	B_{iso}(Co) (Å^2)	x_O	y_O	z_O	B_{iso}(O) (Å^2)	R_{wp} (%)	R_B (%)	R_F (%)
$LaCoO_3$	5.3861(6)	60.7023(8)	0.24(3)	0.28(3)	0.21153(22)	0.28847(22)	0.75	0.78(4)	9.17	4.68	3.73
$La_{0.92}CoO_{2.93}$	5.3646(8)	60.9619(8)	0.26(3)	0.28(4)	0.20927(25)	0.29073(25)	0.75	0.77(5)	10.25	5.33	4.12

dx.doi.org/10.1021/ic200178x |*Inorg. Chem.* 2011, 50, 4412–4416

Zhou et al.,[10] the crystalline quality and transport properties of materials synthesized by the cold high pressure are much better than those of samples synthesized by a conventional solid-state reaction or sol−gel method. Especially, $\rho(T)$ and $\kappa(T)$ in such cold-pressed ceramic samples are nearly the same as those in the single-crystalline counterparts; in contrast, $\rho(T)$ and thermal resistivity $\kappa^{-1}(T)$ in conventional ceramics synthesized by a traditional solid-state reaction or sol−gel method can be up to 1 order of magnitude higher than those in the single-crystalline counterparts. For comparison, we also prepared several samples by a conventional solid-sate reaction (see the Supporting Information). In these samples synthesized by the conventional solid-state reaction, there are numerous pores and cracks as revealed by the SEM image, and the thermal and electric conductivities are much lower than those of the samples synthesized by cold high pressure. In contrast to the solid-state-reaction-synthesized samples, the compact cold-pressed samples have thermal and electric conductivities comparable to those of single crystals.[11,12] The availability of high-density samples allows us to investigate the intrinsic thermal conduction and TE behaviors.

As shown in Figure 2a, the $\kappa-T$ behaviors are similar for all $La_{1-x}CoO_{3-y}$ samples, but the κ values gradually decrease with an increase in the vacancy content. Especially, compared with $La_{1-x}Sr_xCoO_3$, the κ reduction in $La_{1-x}CoO_{3-y}$ is clear (Figure 2b). Estimated from the Wiedemann−Franz law, the phonon thermal conductivity κ_{ph} is dominant in these samples ($\kappa_{ph}/\kappa \geq 90\%$), so the decrease in κ arises mainly from suppression of phonon transport. Because our compact ceramic samples have a κ magnitude comparable to that of single crystals (see Figure 2b),[12] therefore, the grain boundaries in these ceramics have less influence on κ, and thus the introduced La/O vacancies cause an intrinsic suppression of κ. It is surprising that the slight ion deficiencies result in such a noticeable κ reduction. In this $LaCoO_3$ family, the specific heat measurements reveal that $La_{1-x}CoO_{3-y}$ and $La_{1-x}Sr_xCoO_3$ have nearly the same Debye temperature θ_D and average phonon velocity v (see the Supporting Information), but κ in $La_{1-x}CoO_{3-y}$ is less than one-third of that in $La_{1-x}Sr_xCoO_3$. This means that, in addition to phonon−phonon scattering, there exist other phonon scattering mechanisms in $La_{1-x}CoO_{3-y}$ that depress κ. Considering the existence of La/O vacancies that may cause some local anharmonic vibrations (viz., these vacancies might act as "rattlers"),[13] it is reasonable to speculate that point-defect scattering is the most likely mechanism herein. Moreover, such a mechanism is expected to scatter phonons over a wide frequency range, which thus leads to a corresponding decrease in κ over a wide temperature range, as observed. To better understand this scenario, next we compare the observed κ with that predicted by the point-defect scattering theory.

In the point-defect scattering theory, the total scattering rate τ^{-1} is expressed by[14,15]

$$\tau^{-1} = \tau_{pd}^{-1} + \tau_{ph}^{-1} + \tau_b^{-1} \quad (1)$$

where τ_{pd}^{-1}, τ_{ph}^{-1}, and τ_b^{-1} denote the scattering rates for point-defect scattering, phonon−phonon scattering, and boundary scattering, respectively. The boundary scattering is the same and is negligible for all samples; the phonon−phonon scattering gives $\kappa \propto T^{-1/2}$, but here κ increases with temperature, suggesting that τ_{ph}^{-1} is also less important. Therefore, τ_{pd}^{-1} is dominant for all samples, and the different κ values between $La_{1-x}CoO_{3-y}$ and $La_{1-x}Sr_xCoO_3$ originate from their different point-defect scattering.

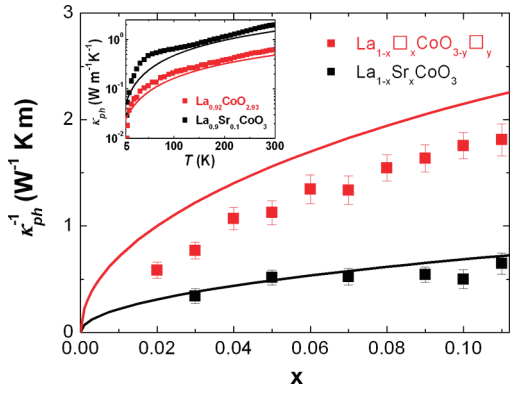

Figure 3. Room temperature phonon thermal resistivity κ_{ph}^{-1} of $La_{1-x}\square_xCoO_{3-y}\square_y$ and $La_{1-x}Sr_xCoO_3$ as a function of the vacancy/Sr content x. The square dots are the experimental data, while the solid lines are the calculated κ_{ph}^{-1} from point-defect scattering theory. Here we assume that $x = y$ in $La_{1-x}CoO_{3-y}$; viz., the La and O vacancies are equal in number. Although y/x is actually ~0.8−1, this assumption does not affect the conclusion. The inset shows $\kappa(T)$ of $La_{0.92}CoO_{2.93}$ and $La_{0.9}Sr_{0.1}CoO_3$, together with the calculation curves by phonon scattering theory proposed by Callaway et al.[14,15]

For a system governed by point-defect scattering, phonon thermal resistivity κ_{ph}^{-1} is given by $\kappa_{ph}^{-1} = 4\pi v(ACT)^{1/2}/k_B$,[15,16] where A and C are characteristic parameters. Parameter C can be determined from the measured κ_{ph} of a pure material in which $\kappa_{pure} = k_B^2\theta_D/2\pi^2v\hbar CT$. Because $La_{1-x}CoO_{3-y}$ and $La_{1-x}Sr_xCoO_3$ have the same θ_D and v [$\theta_D \sim 380$ K from the fitting of specific heat data and $v \sim 2850$ m/s according to $v = (6\pi^2N)^{-1/3}k_B\theta_D/\hbar$], they also have the same parameter C, which is calculated to be 2.27×10^{-17} s/K at 300 K. Parameter A is given by $A = V_0\Gamma/4\pi v^3$, where V_0 is the unit-cell volume and Γ is the scattering parameter. In $La_{1-x}Sr_xCoO_3$, there is only one type of doped ion, Sr, with a relative concentration x, so $\Gamma = x(1 - x)(\Delta M/M_{av})$, where ΔM is the mass difference between Sr and La and M_{av} is the average mass.[16] Thus, the A values for $La_{1-x}Sr_xCoO_3$ can be determined as a function of x. In $La_{1-x}CoO_{3-y}$, the situation is complex because there are no doped ions but both La and O sites have vacancies. Nonetheless, if $La_{1-x}CoO_{3-y}$ is thought of as solid solution $La_{1-x}\square_xCoO_{3-y}\square_y$ consisting of $LaCoO_3$ and $\square_xCo\square_y$, where $\square$ denotes a La vacancy or an O vacancy, the κ behavior can be well understood. For such a ternary compound $P_pQ_qR_r$, the scattering parameter Γ, denoted by $\Gamma(P_pQ_qR_r)$, is given by[17]

$$\Gamma(P_pQ_qR_r) = \frac{p}{p+q+r}\left(\frac{M_P}{M_{av}}\right)^2\Gamma(P) + \frac{q}{p+q+r}\left(\frac{M_Q}{M_{av}}\right)^2\Gamma(Q) + \frac{r}{p+q+r}\left(\frac{M_R}{M_{av}}\right)^2\Gamma(R) \quad (2)$$

where $M_{av} = (pM_P + qM_Q + rM_R)/(p + q + r)$. In the case of $La_{1-x}\square_xCoO_{3-y}\square_y$, P = (La, $\square$), Q = Co, and R = (O, $\square$). Thus, eq 2 can yield an expression of A for $La_{1-x}CoO_{3-y}$. Then, κ_{ph}^{-1} can be calculated for both $La_{1-x}CoO_{3-y}$ and $La_{1-x}Sr_xCoO_3$ by using these parameters and expressions. The calculated plots of κ_{ph}^{-1} at 300 K are shown in Figure 3. The κ_{ph}^{-1} curves predicted by the point-defect scattering theory are consistent with the observed κ_{ph}^{-1} (note that the calculated curves contain no adjustable parameters), which thus accounts well for the experimental κ behaviors; viz., point-defect

dx.doi.org/10.1021/ic200178x |Inorg. Chem. 2011, 50, 4412–4416

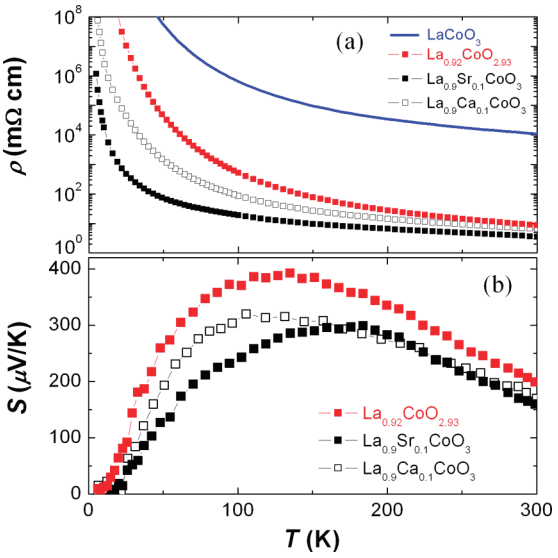

Figure 4. Temperature dependences of (a) resistivity ρ and (b) thermopower S for the samples.

scattering governs the thermal transport in this system. The strong point-defect scattering induced by vacancy □ causes a large κ reduction; namely, the vacancy □ is playing a role as "rattler", which thus strongly scatters phonons. It can also well explain the different κ values between $La_{1-x}CoO_{3-y}$ and $La_{1-x}Sr_xCoO_3$. The mass mismatch between La and □ as well as O and □ is 100%, much larger than that between La and Sr, so the point-defect scattering intensity in $La_{1-x}CoO_{3-y}$ is obviously stronger than that in $La_{1-x}Sr_xCoO_3$. Consequently, $La_{1-x}CoO_{3-y}$ exhibits much lower κ than $La_{1-x}Sr_xCoO_3$. We believe that this scenario can also explain the observed κ reduction in other ion-deficient oxides such as $SrTiO_{3-\delta}$.[18]

The introduced La/O vacancies noticeably reduce κ; however, for TEs, it is also crucial to probe whether these vacancies disturb the electric transport of $La_{1-x}CoO_{3-y}$. As presented in Figure 4, the $\rho-T$ and $S-T$ behaviors in $La_{0.92}CoO_{2.93}$ are similar to those in $La_{0.9}Sr_{0.1}CoO_3$ and $La_{0.9}Ca_{0.1}CoO_3$, and especially the ρ as well as S values are comparable for these samples. This implies that the electric transport properties of the $LaCoO_3$ system are less affected by vacancies overall; instead, they are mainly determined by the Co^{3+}/Co^{4+} ratio. The Hall coefficient measurements show that the room temperature carrier concentrations n for $La_{0.92}CoO_{2.93}$, $La_{0.9}Sr_{0.1}CoO_3$, and $La_{0.9}Ca_{0.1}CoO_3$ are 6.68×10^{21}, 5.61×10^{21}, and 5.32×10^{21} cm^{-3}, respectively, indicating that, although the vacancies provide more free carriers, on the whole, the same Co^{3+}/Co^{4+} ratio gives rise to almost the same carrier concentration. The room temperature ρ values for $La_{0.92}CoO_{2.93}$, $La_{0.9}Sr_{0.1}CoO_3$, and $La_{0.9}Ca_{0.1}CoO_3$ are 8.68, 3.58, and 6.51 mΩ cm, respectively, and the corresponding room temperature carrier mobility μ values are 0.107, 0.313, and 0.181 $cm^2\ V^{-1}\ s^{-1}$. This suggests that the vacancies induce stronger carrier scattering and finally that ρ of $La_{0.92}CoO_{2.93}$ is somewhat higher than those of $La_{0.9}Sr_{0.1}CoO_3$ and $La_{0.9}Ca_{0.1}CoO_3$. Note that their ρ difference is intrinsic because all of the samples have identical microstructure and exhibit ρ comparable to that of single crystals (namely, the influence of grain boundaries is quite small). Considering the different structural distortions in the three systems, their different bandwidth should be responsible for the different ρ values.[9]

On the other hand, S of $La_{0.92}CoO_{2.93}$ is also larger than that of $La_{0.9}Sr/Ca_{0.1}CoO_3$. This is an interesting observation because $La_{0.92}CoO_{2.93}$ has more carriers than $La_{0.9}Sr_{0.1}CoO_3$ and $La_{0.9}Ca_{0.1}CoO_3$, whereas for most semiconductors, the increase in the number of carriers normally reduces S. Thus, herein, the increase in S is derived from another reason than the carrier factor. Such a phenomenon may result for the following two reasons. One reason is that the electronic density of states (DOSs) around the Fermi level, $g(E)$, is increased by introducing vacancies. The specific heat results indeed show that $La_{0.92}CoO_{2.93}$ has a larger electronic specific heat coefficient γ (see the Supporting Information). Because in such an electron-correlated semiconductor system $S \propto \gamma \propto m^* \propto [g(E)]^{2/3}$ (m^* is the electron effective mass),[19] the enhanced electron correlation is responsible for the increase in S. This is also supported by the band calculations on ion-vacant perovskites.[20] The other reason is that the electronic configurations of Co ions may vary in $La_{0.92}CoO_{2.93}$. It is well-known that there exist rich spin states in the $LaCoO_3$ system and the crossover between the different spin states sensitively depends on the crystal structure and Co−O bond length.[21] As mentioned above, the XRD data reveal that $La_{1-x}CoO_{3-y}$ exhibits a contraction of its lattice, which may cause some variations in the spin state of Co ions and thus change the configurational entropy of the system. Because the configurational entropy is quite important in determining S in cobalt oxides,[22] variations in electronic configurations will also influence S. Further investigations are needed to clarify the origin of the observed S enhancement, but those are beyond the scope of the present study.

Because of the large κ reduction, ZT in the La/O-vacant samples is efficiently improved. Compared with the highest ZT in $La_{1-x}Sr_xCoO_3$ ($ZT \sim 0.1$ at 300 K),[9] the room temperature ZT exceeds 0.18 in $La_{0.92}CoO_{2.93}$, which is nearly doubled. It is noteworthy that herein the ZT enhancement has nothing to do with sample morphologies, so further ZT improvement is likely by a conjunction of nanoengineering and the mechanism described in this study. We have shown that the compact $La_{1-x}Sr_xCoO_3$ nanowires exhibit twice the value of ZT compared with the ceramic counterparts,[23] so it might be estimated that $ZT \sim 0.4$ around 300 K for nanosized $La_{1-x}CoO_{3-y}$.

CONCLUSION

In summary, we present a systematic study on the thermal conductivity and TE properties of a series of La/O-vacant $La_{1-x}CoO_{3-y}$. In these $La_{1-x}CoO_{3-y}$ samples, κ is strongly suppressed by the La/O vacancies, whereas ρ and S depend mainly on the Co^{3+}/Co^{4+} ratio and they are less affected by the vacancies. As a result, $La_{1-x}CoO_{3-y}$ shows an efficiently improved TE performance. Such intrinsic κ suppression may be achieved in various oxide systems and can work in conjunction with other phonon engineering such as nanostructuring, so it could be very useful for the design of better TE materials.

ASSOCIATED CONTENT

Supporting Information. Details of the EDS, XPS, and specific heat results and the microstructure as well as transport properties of samples prepared by a conventional solid-state reaction. This material is available free of charge via the Internet at http://pubs.acs.org.

AUTHOR INFORMATION

Corresponding Author

*E-mail: wang_yang@ntu.edu.sg (Y.W.), suiyu@hit.edu.cn (Y.S.).

REFERENCES

(1) Ohta, H.; Sugiura, K.; Koumoto, K. *Inorg. Chem.* **2008**, *47*, 8429.
(2) Koumoto, K.; Wang, Y. F.; Zhang, R. Z.; Kosuga, A.; Funahashi, R. *Annu. Rev. Mater. Res.* **2010**, *40*, 363.
(3) Terasaki, I.; Sasago, Y.; Uchinokura, K. *Phys. Rev. B* **1997**, *56*, 12685.
(4) Takahata, K.; Iguchi, Y.; Tanaka, D.; Itoh, T.; Terasaki, I. *Phys. Rev. B* **2000**, *61*, 12551.
(5) (a) Ohta, S.; Nomura, T.; Ohta, H.; Hirano, M.; Hosono, H.; Koumoto, K. *Appl. Phys. Lett.* **2005**, *87*, 092108. (b) Liu, J.; Wang, C. L.; Su, W. B.; Wang, H. C.; Zheng, P.; Li, J. C.; Zhang, J. L.; Mei, L. M. *Appl. Phys. Lett.* **2009**, *95*, 162110.
(6) Iwasaki, K.; Ito, T.; Nagasaki, T.; Arita, Y.; Yoshino, M.; Matsui, T. *J. Solid State Chem.* **2008**, *181*, 3145.
(7) Boukai, A. I.; Bunimovich, Y.; Kheli, J. T.; Yu, J. K.; Ill, W. A. G.; Heath, J. R. *Nature* **2008**, *451*, 168.
(8) Poudel, B.; Hao, Q.; Ma, Y.; Lan, Y. C.; Minnich, A.; Yu, B.; Yan, X.; Wang, D. Z.; Muto, A.; Vashaee, D.; Chen, X. Y.; Liu, J. M.; Dresselhaus, M. S.; Chen, G.; Ren, Z. F. *Science* **2008**, *320*, 634.
(9) Wang, Y.; Sui, Y.; Ren, P.; Wang, L.; Wang, X. J.; Su, W. H.; Fan, H. J. *Inorg. Chem.* **2010**, *49*, 3216.
(10) Zhou, J. S.; Goodenough, J. B.; Dabrowski, B. *Phys. Rev. B* **2003**, *67*, 020404R.
(11) Kriener, M.; Zobel, C.; Reichl, A.; Baier, J.; Cwik, M.; Berggold, K.; Kierspei, H.; Zabara, O.; Freimuth, A.; Lorenz, T. *Phys. Rev. B* **2004**, *69*, 094417.
(12) Berggold, K.; Kriener, M.; Zobel, C.; Reichl, A.; Reuther, M.; Müller, R.; Freimuth, A.; Lorenz, T. *Phys. Rev. B* **2005**, *72*, 155116.
(13) Sales, B. C.; Mandrus, D.; Chakoumakos, B. C.; Keppens, V.; Thompson, J. R. *Phys. Rev. B* **1997**, *56*, 15081.
(14) Callaway, J. *Phys. Rev.* **1959**, *113*, 1046.
(15) Callaway, J.; von Baeyer, H. C. *Phys. Rev.* **1960**, *120*, 1149.
(16) Klemens, P. G. *Phys. Rev.* **1960**, *119*, 507.
(17) Slack, G. A. *Phys. Rev.* **1962**, *126*, 427.
(18) Yu, C.; Scullin, M. L.; Huijben, M.; Ramesh, R.; Majumdar, A. *Appl. Phys. Lett.* **2008**, *92*, 191911.
(19) Snyder, G. J.; Toberer, E. S. *Nat. Mater.* **2008**, *7*, 105.
(20) Wunderlich, W.; Ohta, H.; Koumoto, K. *Physica B* **2009**, *404*, 2202.
(21) Takami, T.; Zhou, J. S.; Goodenough, J. B.; Ikuta, H. *Phys. Rev. B* **2007**, *76*, 144116.
(22) Koshibae, W.; Tsutsui, K.; Maekawa, S. *Phys. Rev. B* **2000**, *62*, 6869.
(23) Wang, Y.; Fan, H. J. *J. Phys. Chem. C* **2010**, *114*, 13947.